Aerodynamics and Optimization of Airfoil Under Ground Effect

Kyoungwoo Park, Byeong Sam Kim, Juhee Lee, and Kwang Soo Kim

Abstract—The Prediction of aerodynamic characteristics and shape optimization of airfoil under the ground effect have been carried out by integration of computational fluid dynamics and the multi-objective Pareto-based genetic algorithm. The main flow characteristics around an airfoil of WIG craft are lift force, lift-to-drag ratio and static height stability (*H.S*). However, they show a strong trade-off phenomenon so that it is not easy to satisfy the design requirements simultaneously. This difficulty can be resolved by the optimal design. The above mentioned three characteristics are chosen as the objective functions and NACA0015 airfoil is considered as a baseline model in the present study. The profile of airfoil is constructed by Bezier curves with fourteen control points and these control points are adopted as the design variables. For multi-objective optimization problems, the optimal solutions are not unique but a set of non-dominated optima and they are called Pareto frontiers or Pareto sets. As the results of optimization, forty numbers of non- dominated Pareto optima can be obtained at thirty evolutions.

Keywords—Aerodynamics, Shape optimization, Airfoil on WIG craft, Genetic algorithm, Computational fluid dynamics (CFD).

I. INTRODUCTION

ACCORDING to the IMO[1], a WIG (wing-in-ground effect) craft is defined as a transport that has fixed wings like an airplane and has the advantages of increasing lift and decreasing drag when it flies above the water or ground surface at a sufficiently low level. WIG crafts operate close to the water or ground surface (i.e., at a height of 30 % of its chord length or lower) by utilizing an air cushion of relatively high pressurized air between airfoil and ground. Due to the air cushion, lift augmentation and drag reduction are considerable over against an airfoil out of ground effect. No fast ship can match the speed of a WIG craft and no economical aircraft can match the operational expenses of a WIG craft. Therefore, WIG crafts being in the niche between ships and aircrafts can be alternative means of next-generation transportation in the near future.

In spite of many advantages, a WIG craft has technical difficulties to overcome such as the hump drag, which is a main

factor for the disturbance of high speed to take off above the surface, and the instability problem, which is not generally observed in a typical airplane. Generally, the cambered airfoil, which can get additional lift by ground effect, is difficult to satisfy the static height stability (*H.S*)[2]. Until quite recently, the researches on the WIG craft had mostly concentrated on the aerodynamic characteristics experimentally and/or numerically. Kikuchi et al.[3] measured the interaction forces on the airfoil and compared their results with numerical ones. Joh et al. [4] studied numerically on the pressure change, drag and stability around an airfoil of the WIG crafts. Kim and Joh [5] obtained the optimized airfoil shape by using the single-objective optimization technology. They said that the lift coefficient was improved by 5.6 percent compared with the DHMTU airfoil although the *H.S.* had almost the same value. Im and Chang [6] investigated the aerodynamic characteristics of NACA4415 with a cambered airfoil under the free-flight conditions. They showed that the lift-to-drag ratio of NACA4415 is slightly increased as the air craft is approaching to the ground. They also found that the pressure is increased at the leading edge only for the case of small angle of attack. Optimal design of the WIG airfoil was studied by only a few researchers. Most of them treated the single objective optimization with the local optimization technique. Kim and Chun [7] performed the computational optimization for airfoil shape. They chose the pressure distributions and lift coefficient as the objective functions and obtained the optimal solutions by using a gradient-based local optimization technologies.

In this study, in order to obtain the best airfoil profile under the influence of ground effect, the shape optimization is performed by integrating the computational fluid dynamics (CFD) and global optimization technology such as the multi-objective genetic algorithm (MOGA). Lift coefficient, lift-to-drag ratio and *H.S.*, which mainly influence the performance of WIG craft, are adopted as objective functions. The airfoil shape is parameterized by Bezier-curves and their control points are used as the design variables. Due to the peculiarity of the tradeoffs between conflicting objective functions, a number of individuals which are not dominated by the other ones within the design space can be obtained and the non-dominated optimal solutions are Pareto frontier (or sets).

II. MATHEMATICAL MODEL

2.1. Physical Model for Airfoil

A schematic configuration and a coordinate system of

World Academy of Science, Engineering and Technology
International Journal of Aerospace and Mechanical Engineering
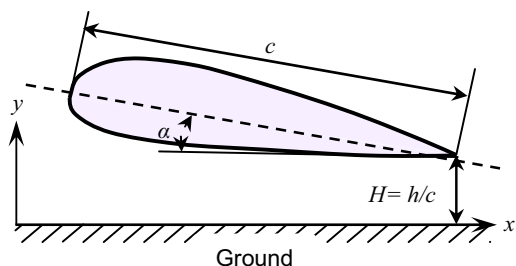Vol:3, No:4, 2009

Fig. 1 Physical model and coordinate system of airfoil

airfoils in WIG craft considered in this study are shown in Fig. 1. The flow around an airfoil is assumed to be turbulent and steady state with incompressible fluid. The turbulent flow of air is described by the Reynolds-Averaged Navier-Stokes (RANS) equations and it can be expressed in tensor notation for mass and momentum as follows:

$$\frac{\partial}{\partial x_j}\left(\rho u_j\right) = 0 \tag{1}$$

$$\frac{\partial}{\partial x_j}\left(\rho u_j u_i - \tau_{ij}\right) = -\frac{\partial p}{\partial x_i} + s_i \tag{2}$$

$$\tau_{ij} = \mu_t S_{ij} - \frac{2}{3}\mu_t \frac{\partial u_k}{\partial x_k}\delta_{ij} - \rho\overline{u_i' u_j'} \tag{3}$$

where x_j, $j = 1, 2, 3$ are the Cartesian coordinate vector, u_j the mean velocity components. $-\rho\overline{u_j' u_i'}$ the Reynolds stress tensor. μ_t and S_{ij} are the turbulent viscosity and the modulus of the mean strain rate tensor which are defined, respectively, as

$$\mu_t = f_\mu \cdot C_\mu \frac{\rho k^2}{\varepsilon}, \quad S_{ij} = \left(\frac{\partial u_i}{\partial x_j} + \frac{\partial u_j}{\partial x_i}\right) \tag{4}$$

In the present study, the RNG $k - \varepsilon$ model proposed by Yakhot et al. [8] is applied to model the turbulent flow around the airfoil. It is known that the RNG $k - \varepsilon$ model included an additional term in its ε-equation can significantly improve the accuracy for airfoil flows.

2.2. Numerical Method for Flow Analysis

In order to avoid the blockage effects and disturbances of outer boundaries, the computational domains are extended as follows; the inlet region is far from the leading edge by *10c* (*c* is the chord length of airfoil) and the exit in downstream direction is located at the distance of *20c* from the trailing edge. The top outer boundary of *y*-direction is extended by *10c* from the upper crest location. For calculating the objective functions for shape optimization (i.e., lift, lift-to-drag ratio and *H.S.*), a commercial S/W, STAR-CD [9], is used in this study because most of the computational cost for optimization is consumed when objective functions are evaluated. Therefore, the cost effective and high fidelity RANS solver for turbulent flow should be required. For the treatment of convective and diffusion terms in governing equations, the second order

upwind and central differencing schemes are adopted, respectively. The pressure-velocity coupling is resolved using the SIMPLE algorithm [10]. The accuracy and efficiency of computational results are also dependent on how the grid system is constructed. For the purposes of the accurate and effective computation, mixed type of O-type and H-type grid are used in this study. Especially 20 layers of O-type grids for the boundary layer development are employed next to the airfoil. The present computation is carried out for Reynolds number of 2.8×10^6 based on the airfoil chord(*c*) and the corresponding inlet velocity of 34.28 *m/s*. No-slip boundary condition on airfoil surface, moving wall boundary at the ground and pressure boundary condition at the exit (*x*-direction) are employed. The slip-wall boundary condition is prescribed at the top-outer boundary. The solutions are considered to be converged when all of the residuals for the continuity and momentum equations are less than or equal to 10^{-6}. For the calculation of *H.S.*, that is one of the objectives, derivatives with respect to height and angle of attack are required so that five times of CFD calculation is required to evaluate one design. Overall computational time to complete the optimization process is about 187 hours (about 8 days). To minimize the computational time, previous computational results are stored and when a new evaluation is required, the optimizer searches the storage first and then begins a new evaluation.

III. Optimization

Many optimization technologies have been developed to obtain the optimal solutions for various industrial applications. Among them, gradient-based methods such as a SQP and SLP are well-known techniques that seek to find the optimum using local gradient information so that the optimum obtained from these methods may be a local one. Especially, to treat the multi-objective optimization one, they convert it into a single objective optimization problem using a weighted sum of all the objective functions with a normalization technique. However, it may distort the original design space and lead to get the solution of local optima. In addition, when orders of magnitude among the objectives are significantly different, they tend to focus on the biggest one. The normalization can also give some resolves but basically, the distortion might be still remained.

In order to avoid the characteristics of gradient-based methods, the multi-objective GA, simply called it as MOGA, is introduced to find the global optima and it is attractive for airfoil shape optimization having multi-objectives. The optimal solutions of the multi-objective problem cannot be defined uniquely except for the linearly dependent system. All designs can be classified into dominated and non-dominated ones. The latter is called a Pareto set which is located on the front line of the design space. Generally, the Pareto optima cannot be improved upon without mischief of at least one of the solutions.

3.1. Concept of Pareto frontier (or set)

World Academy of Science, Engineering and Technology
International Journal of Aerospace and Mechanical Engineering
Vol:3, No:4, 2009

A multi-objective optimization does not look for a unique solution but a set of ones. Thus, all these solutions belong to a hyper-surface and this locus of optimal solutions is called the tradeoff surface between conflicting objective functions or the Pareto frontier. From the Pareto frontier point of view, none of the optima are dominated. This indicates that none of the objectives can be improved without worsening of at least one of the other objectives. For explaining the Pareto frontier, a multi-objective problem with m-objective functions to be minimized is considered. The individual **A** dominates with respect to the individual **B** if, for at least one of the objectives, the values of objective function for **A** are strictly better than those of **B** and if, for all other objectives, **A** is not worse than **B**. According to this definition, an individual will be considered as Pareto optimal if it is non-dominated. Mathematically, **B** is Pareto optimal if there does not exist another individual **A** as follows,

$$\mathbf{A}_P > \mathbf{B} \Leftrightarrow \left[\forall i \in \{1, \cdots m\} \quad F_i(\mathbf{A}) \leq F_i(\mathbf{B}) \right]$$
$$\cap \left[\exists i \in \{1, \cdots m\} \, F_i(\mathbf{A}) < F_i(\mathbf{B}) \right] \qquad (5)$$

3.2. Multi-Objective Genetic Algorithm (MOGA)

The genetic algorithm is a unique global optimum algorithm based on the survival of the fittest, the mechanism of natural selection and reproduction [11, 12, 13]. Each individual has the number of strings representing characteristics of an individual design instead of the gene in natural life. One generation consists of a group of individuals. For the evolution of solutions, new individuals for the next generation can be obtained by using genetic operations such as selection, crossover, mutation, and niche. The selection introduces the direction of the evolution for the survival of the fittest and decides parents from the genetic pool. The crossover is a process reproducing the superior individuals to evolve the generation globally. Since crossover and selection only rearranging the genes are deterministic processes, it is difficult to introduce completely new genes, which did not exist previously. The deficiency of searching design space leads a lot of danger to converge into the local optima after all. The mutation can prevent the deficiency and keep GA's balance to find the global optima. Balanced searching between crossover and mutation can effectively lead the GA to the global optima. Differently from the random search, these genetic operations can improve the average fitness of a generation constantly. The properties of adjacent individuals in the design space are similar to each other. For extending exploration, it is necessary to control the number of individuals inside the niche radius. Before sufficient exploration or at an early stage of evolution, the existence of local optima is very attractive. The offspring tends to gather around the local optimum points, which lead early mature convergence. The niche is able to give a change to explore the design space and prevent GA from early mature convergence. In this study, the binary distance between two individuals instead of the n dimensional norm as the niche distance is employed.

$$\frac{r_{ij}}{R} = \sum_{k=1}^{L} \left[\frac{\left| d_i - d_j \right|}{R} \right]_k = \sum_{k=1}^{L} \left[\frac{m \cdot \Delta x}{n \cdot \Delta x} \right]_k = \sum_{k=1}^{L} \left[\frac{m}{n} \right]_k \qquad (6)$$

where $\left| d_i - d_j \right|_k$ is the distance between i and j individual in k variable, m the binary distance and n the niche binary distance. It is difficult to presents all niche at once in real design space by the niche radius, so that the niche radius for each design variable is required. For the case of the binary distance, however, one niche radius is sufficient.

IV. RESULTS AND DISCUSSION

In this study, the optimal solutions for the airfoil of WIG craft are numerically obtained. A numerical analysis is automatically performed under the control of the optimizer to evaluate the objectives such as the aerodynamic forces and static height stability and NACA0015 profile is used as a baseline model for the optimization. The MOGA is used as an optimizer so that a normalization process and a weighting technique for solving the multi-objective problems are not needed. The optimization is performed under the normal cruise state such as $h/c = 0.25$ (non-dimensional height), and $\alpha = 2^o$ at $\mathrm{Re} = 2.8 \times 10^6$.

4.1. Mathematical Formula for Optimization

Optimization is to find the best values of the design variables that minimize and/or maximize the objective functions while satisfying the constraints and bounds. Thus, optimization problems comprise the following ingredients; design variable(s), objective function(s), constraint(s), and side constraint(s).

Mathematical formula for multi-objective optimization: For WIG craft the optimized airfoil can diminish drag and augment lift due to the ground effect at the same time. However, these favorable phenomena can give rise to the stability problem. Thus, the lift-to-drag ratio, $F_1(\mathbf{X})$, lift coefficient, $F_2(\mathbf{X})$, and static height stability (*H.S.*), $F_3(\mathbf{X})$, are considered as the objective functions in this study.

Find the *control points,* $\qquad \mathbf{X} = \{v_1, v_2, \cdots, v_{18}\}^T \qquad (7)$

to maximize the *lift-to-drag ratio,* $\quad F_1(\mathbf{X}) = C_l / C_d \quad (8a)$

to maximize the *lift,* $\qquad F_2(\mathbf{X}) = C_l \qquad (8b)$

to minimize the *height stability(H.S.)*

$$F_3(\mathbf{X}) = H.S. = C_{l,h} - \frac{C_{m,h}}{C_{m,\alpha}} C_{l,\alpha} \qquad (8c)$$

Subjected to bounds, $X_i^L \leq X_i \leq X_i^U$ for $i = 1,18 \qquad (9)$

Design variables and Constraints: A wide variety of methods for representing an airfoil shape have been introduced. One of the most popular methods is that of the Bezier curve using control points to define airfoil shapes because it generally offers a direct control of the coordinates of control points and it always passes through the first and last control points and lies

World Academy of Science, Engineering and Technology
International Journal of Aerospace and Mechanical Engineering
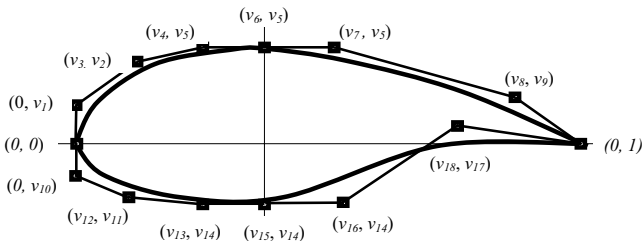Vol:3, No:4, 2009

Fig. 2 Airfoil geometry parameterization

within the convex hull of the control points which leads the smooth change of airfoil shapes. In the present work, the airfoil has been parameterized by four Bezier polynomials: two 4th-order Bezier curves for the leading edge, and two 3rd-order for the trailing edge. A Bezier curve can be represented as follows:

$$\vec{P}(t) = \sum_{i=0}^{k} \vec{P_i} B_{i,k}(t) \quad t \in [0,1] \tag{10}$$

$$B_{i,k}(t) = \frac{k!}{i!(k-i)!} t^i (1-t)^{k-i} \tag{11}$$

where $\vec{P_i}(t)$ is the coordinates of control point, the parameter t is bounded from 0 to 1, and $B_{i,k}$ is the blending function. Figure 2 shows the schematic diagram of WIG airfoil using the Bezier-curve. As shown in Fig. 2, the airfoil shape can be completed by 6 control points on each side of the airfoil. Except for continuous or fixed points such as maximum thickness (v_5), smooth leading edge (v_1, v_{10}) and trailing edge, the number of design variables becomes 18. The three-control points near the maximum thickness have the same height and it guarantees a smooth airfoil profile. Generally, the choices of range and resolution for the design variables are very important factors. Therefore, the pre-optimizations of two times are performed in order to decide the upper and lower limits of design variables properly. Because there is no sufficient information for the design space at the first pre-optimization, the upper and lower bounds based on a base model are extended arbitrarily until avoiding the intersection of control points. Once the Pareto set is obtained from the preliminary optimization, the bounds of the design variables are modified. When optima are

TABLE 1 UPPER AND LOWER LIMITS OF THE DESIGN VARIABLES

X_i	X_i^L	X_i^U	X_i	X_i^L	X_i^U
v_1	0.01	0.04	v_{10}	-0.04	-0.02
v_2	0.05	0.07	v_{11}	-0.07	-0.035
v_3	0.05	0.065	v_{12}	0.035	0.05
v_4	0.08	0.2	v_{13}	0.1	0.2
v_5	0.075	0.1	v_{14}	-0.065	-0.02
v_6	0.22	0.4	v_{15}	0.25	0.35
v_7	0.55	0.75	v_{16}	0.37	0.55
v_8	0.01	0.025	v_{17}	-0.01	-0.03
v_9	0.8	0.95	v_{18}	0.7	0.85

TABLE II PARAMETERS FOR GENETIC ALGORITHM

	Values
Population	30
Generation	25
Cross over rate	0.8
Mutation rate	0.5%
Tournament level	2
Niche binary radius	1

concentrated in the vicinity of one point, the range of the design variable is reduced. From this methodology, relatively high resolution with the same number of bits can be obtained. All the bounds of design variables are listed in Table 1.

Optimization Parameters of MOGA : The optimization parameters used in this study are listed in Table 2. Twenty-five individuals for one population are used and the selection pressure is adopted as 2 to enhance the convergence rate. In each tournament, two candidates are randomly selected from the current generation, and through two competitions, the winner has a chance to become a parent for the reproduction. The number of cutting lines exchanging gene for crossover operation are important. In this study, two cutting lines are used to maximize the life of schema. To prevent a random search and keep the balance between exploitation and exploration, 0.5% of mutation rate is chosen. When a new offspring individual is found to be a genetic twin in the next generation, the individual is ignored, and one more individual will be generated.

4.2 Flow Characteristics of Base Model

The flow field around an airfoil (NACA0015) is considerably altered under the influence of ground effect. Figure 3 depicts the details of pressure distributions around the airfoil in- and out of ground effects (IGE and OGE) at $\alpha = 0^o$ and $Re = 2.8 \times 10^6$. For the case of IGE, the height (h/c) is 0.2. OGE means that an airfoil is placed far away from the ground (i.e., at least $h/c > 0.5$). Lifts of airfoil for IGE and OGE are predicted as -0.321 and 0.0 respectively. In the case of OGE,
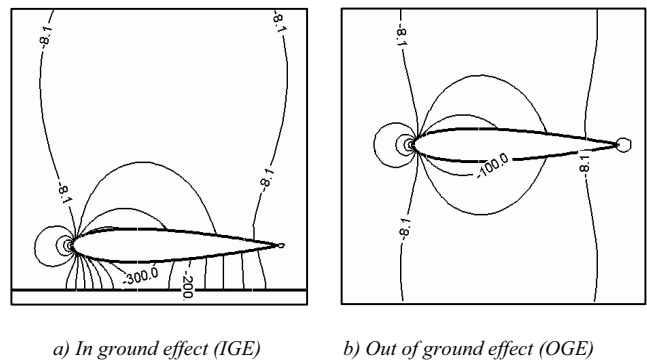

a) In ground effect (IGE) b) Out of ground effect (OGE)

Fig. 3 Pressure distributions around an airfoil with and without ground effects at $\alpha = 0^o$

World Academy of Science, Engineering and Technology
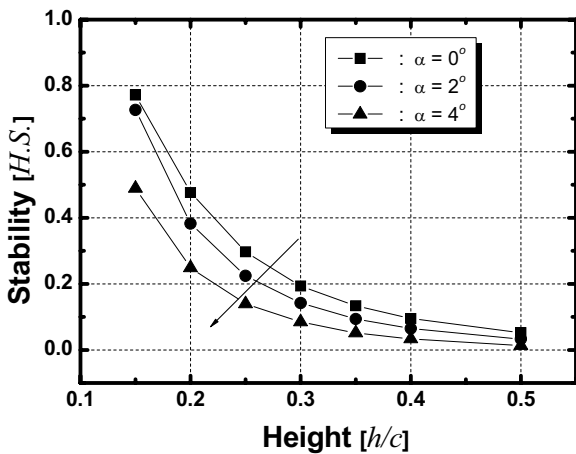International Journal of Aerospace and Mechanical Engineering
Vol:3, No:4, 2009

Fig. 4 Static stability of NACA0015 according to the height (*h/c*) for various angles of attack

pressure on the upper and lower surface is balanced and virtual lift does not exist. However, for IGE, the pressure distribution at the lower side of airfoil is very different from that of OGE and it has a very low value as shown in Fig. 3. This difference on the lower surface can be simply explained from the difference in dynamic pressure at the divergence-convergence passage between airfoil and ground. On the other hand, it is shown that the pressure distributions over the upper surface of airfoil are the same for the both cases.

The static height stability for a base model as a function of height (*h/c*) for various angles of attack (*α*) is shown in Fig. 4. It can be seen in the figure that *H.S.* is increased exponentially with decreasing the height and it causes to decrease the stability. Figure 4 also shows that when the angles of attack are increased, the stability is improved somewhat because of an increase in the ground effect and a decrease in the effect of the convergence- divergence passage. However, all of static height stabilities are larger than zero and not satisfied at any heights and angles of attack. This implies that a symmetric airfoil such as a base model (NACA0015), which was designed without considering the ground effect, is not adequate to that of WIG craft unquestionably.

4.3 Optimal solutions

It is clear that both C_l and C_l/C_d are maximized while *H.S.* is minimized, simultaneously, for obtaining the best performance of WIG craft. This implies that the optimum solution is not a unique one but a set of numerous non-dominated solutions. For the optimization of airfoil shapes in WIG craft, the shape of NACA0015 airfoil is used as a baseline model and flow characteristics (or objective functions) such as lift, lift-to-drag ratio and *H.S.* are calculated by CFD solver.

In the present work, the minimized and maximized objective functions are lift, lift-to-drag ratio and *H.S.* and then the optimal solutions should be displayed in three-dimensional space (that is, C_l, C_l/C_d and *H.S.*). However, it is hard to explain their relationship and features of each function in one 3-dimensional figure so that all individuals are projected into

two-dimensional design space instead of three-dimensional one as shown in Figs. 5 - 7. The hollow squares represent the Pareto frontiers while the filled squares stand for the dominated solutions in these figures.

Pareto optima and dominated individuals between the lift and lift-to-drag are displayed in Fig. 5. It is clear that Pareto
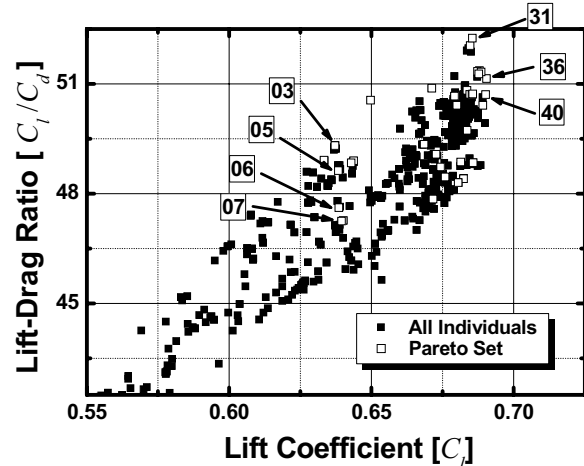

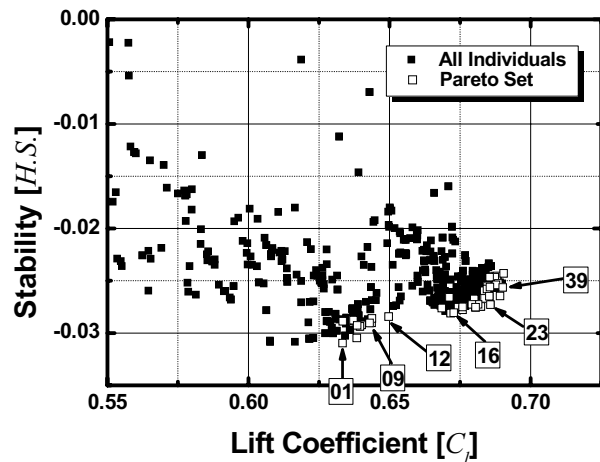Fig. 5 Pareto set and dominated individuals for C_l and C_l/C_d

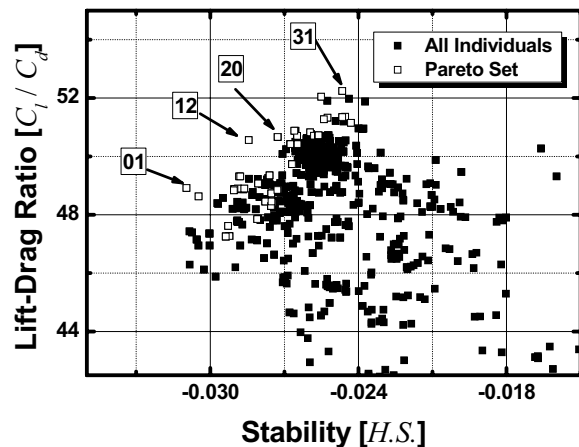Fig. 6 Pareto set and dominated individuals for *H.S.* and C_l

Fig. 7 Pareto sets and dominated individuals for *H.S.* and C_l/C_d

World Academy of Science, Engineering and Technology
International Journal of Aerospace and Mechanical Engineering
Vol:3, No:4, 2009

sets (i.e. Pareto # 31, 36 and 40) for these two objectives are placed at the top-right corner and others are located behind the Pareto frontier line since two objective functions (C_l and C_l/C_d) should be maximized. Individuals in the projected graph of lift and lift-to-drag ratio fall into a narrow and long line. Fig. 5, which plots only small part of the whole graph, shows that the lift coefficient and lift-to-drag ratio are linearly dependent but slightly affected by local drag. Some Pareto optima (Pareto # 03, 05, 06 and 07) can be observed in the area behind frontier line in which some dominated individual are exited. This inconsistency comes from the projection of three-dimensional design space onto two-dimensional one.

Figure 6 shows the Pareto sets for the lift and static height stability. Because the Pareto sets are moved in the direction of minimizing *H.S.* and maximizing lift, they are mostly placed around the bottom-right corner. Pareto#01 means that the design variables are changed in order to minimize *H.S.* whereas Pareto#39 maximizes lift. Note that the values of C_l and *H.S.* for a baseline model (NACA0015) are calculated as 0.135 and 0.224, respectively, and they cannot be displayed because of out of range in Fig. 6. It implies that the aerodynamic characteristics around the NACA0015 airfoil are highly different from those of optimized airfoil shape.

Figure 7 depicts all individuals including the Pareto sets for *H.S.* and C_l/C_d. As discussed earlier, C_l/C_d is inversely proportional to *H.S.* because the former is maximized and the latter is minimized. It can be seen in Fig. 7 that the Pareto sets can be classified into two parts; if the lift-to-drag ratio is superior to the stability in the Pareto sets, they are located at the top-middle side (i.e., Pareto#31) and for the opposite case, the Pareto sets are placed at the lower-left corner (i.e., Pareto#01). Therefore, it can be readily understood that two objective functions (i.e., C_l/C_d and *H.S.*) are conflicted with each other so that improving one of them can deteriorate another of necessity.

Table 3 shows the results of correlation analysis, correlation and p-value (probability value), between the design variables and objective functions. Design variables for leading edge and maximum thickness point not only guide oncoming air into the region between the airfoil and ground but also are aerodynamically very important. By analysis of correlations with 95% reliability, similar results can be obtained; v_4, v_5, v_6 and v_{11} have a direct proportion with objectives. v_5 and v_6 represent the value of maximum thickness and its location,

TABLE III CORRELATION AND *P*-VALUES FOR VARIABLES AND OBJECTIVES

Variable No.		v_4	v_5	v_6	v_{11}
C_l	Correlation	0.458	0.970	03824	-
	p-value	0.003	0.000	0.015	-
H.S.	Correlation	0.452	0.779	0.513	0.533
	p-value	0.003	0.000	0.001	0.000
C_l/C_d	Correlation	0.625	0.476	0.613	0.680
	p-value	0.000	0.002	0.000	0.000

TABLE IV OPTIMAL DESIGN VARIABLES AND OBJECTIVE FUNCTIONS FOR SELECTED PARETO SETS

No. of Pareto	Design variables (selected)				Objective function		
	v_4	v_5	v_6	v_{11}	C_l	C_l/C_d	*H.S.*
#01	0.177	0.085	0.238	-0.052	0.63	48.20	-0.031
#12	0.189	0.088	0.322	-0.048	0.65	50.55	-0.028
#20	0.174	0.097	0.322	-0.052	0.68	50.67	-0.027
#31	0.177	0.097	0.322	-0.036	0.69	52.25	-0.025
NACA 0015	0.15	0.075	0.3	-0.057	0.14	8.361	0.225

respectively. v_4 and v_{11} indicate the leading edge of upper and lower surface. The corresponding values of the objective functions and selected design variables for Pareto#01, #12, #20 and #31 are compared with those of a baseline model (NACA0015) and displayed in Table 4. Table 4 shows that the aerodynamic performance of all optimal solutions is significantly improved compared with that of a baseline model (for example, the lift force (C_l) is increased and *H.S.* is decreased dramatically). For the case of optimal solution of Pareto#31, it is clear that the shape of lower surface is thinner and flatter at the leading edge than that of Pareto#01(i.e., the location of v_{11} for Pareto#31 approaches the chord line. The values of v_{11} for Pareto#01 and 31 are -0.052 and -0.036, respectively). This shape change brings about the variation of pressure distribution on the lower wing surface in order to increase the lift force due to the ram effects at this region. On the contrary, as can be seen in the change of v_5 location (*y*-direction), the upper surface of airfoil is thickened to increase the lift force. For the Pareto#01 point of view, all results will be explained conversely.

The pressure distributions (C_p) and the airfoil profiles for selected Pareto optima are shown in Fig. 8. Pressure distributions of each Pareto optimum depend on the airfoil configuration (location of maximum thickness and curvature of around leading edge). One interest thing is that all profiles on the lower surface of Pareto optima are parallel with ground
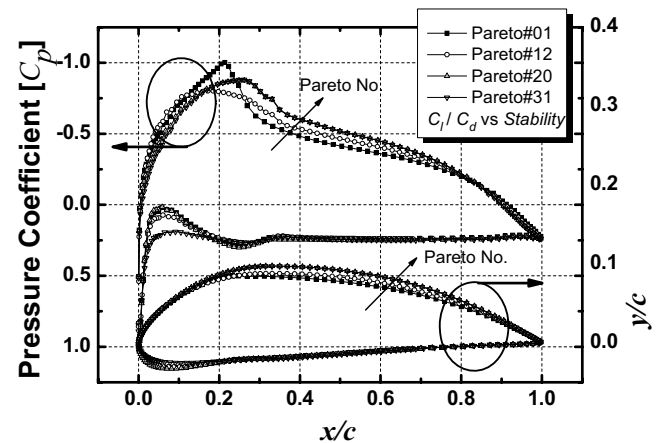

Fig. 8 Profiles and *Cp* of Pareto sets for *H.S.* and C_l/C_d

World Academy of Science, Engineering and Technology
International Journal of Aerospace and Mechanical Engineering
Vol:3, No:4, 2009

except for the leading edge. This flat lower surface can be explained by maximizing stagnation of oncoming air which increases lift as well as decreases drag simultaneously. The same results (i.e. flatness in lower surface) can be observed in previous experimental studies [15, 16]. They suggested the modified Glenn Martine 21 airfoil with a flat surface after $x/c = 0.3$ which is maximized the ground effect and improve aerodynamic characteristics. It is very important to understand the physics on the effect of optimized airfoil shape on the improvement of aerodynamic performances of WIG craft (i.e., increase in lift and decrease in drag forces). Drag force in 2-dimensional flow generally arises from both friction and pressure which comes from a shear stress on the wetted airfoil surface and a pressure distribution on airfoil surface, respectively, while lift force is created by the pressure difference between upper and lower sides of airfoil.

V. CONCLUSIONS

The shape optimization of airfoil under the ground effect was carried out by integration of CFD and multi-objective Pareto-based genetic algorithm (MOGA). Before the optimization was performed, a numerical simulation for prediction the aerodynamic characteristics of NACA 0015 airfoil, which is used as a baseline model, was conducted and this symmetric airfoil experienced negative lift force when it approaches to the ground. From this result, it is clear that the symmetric airfoil such as NACA015 was not adequate for that of WIG craft. The design variables were parameterized by using the Bezier-curve and the pre-optimization process was performed by three times in order to determine the lower and upper limits of design variables. The multi-objective optimization problem was solved using the MOGA without weighting factors and normalization processes. From the analysis of these Pareto optima which include various airfoil sections, aerodynamic characteristics and *H.S.* are explored. Two objectives, C_l and C_l / C_d, projected to a 2-dimensional plot are linearly dependent on each other. The airfoil profiles of the lower side become flat and are almost alike for all Pareto optima. This airfoil shape can prevent the venturi effect which is generally observed in a base model and can improve the ram effect. These phenomena may help to reduce the drag and increase the lift simultaneously. Pareto optima improve the lift and lift-drag ratio by about 5 and 6 times, compared with a base model respectively. *H.S.* values for Pareto optima are satisfied the stability condition. As a result, the WIG craft with the airfoil profiles obtained from the multi-objective optimization technique are more stable and have a high performance compared to those of a base model.

REFERENCES

[1] http://www.imo.org/home.asp
[2] Rozhdestvensky KV. Wing-in-ground effect vehicles. Progress in Aerospace Sciences 2006; 42: 211-283.
[3] Kikuchi K, Motoe F, Yanagizawa M. Numerical Simulation of the Ground Effect Using the Boundary Element Method. International Journal For Numerical Methods in Fluids 1997; 25: 1043-1056.
[4] Joh CY, Kim YJ. Computational Aerodynamic Analysis of Airfoils for WIG (Airfoil-In-Ground-Effect)-Craft. Journal of the Korean Society for Aeronautical and Space Sciences 2004; 32 (8): 37-46.
[5] Kim YJ, Joh CY. Aerodynamic Design Optimization of Airfoils for WIG Craft Using Response Surface Method. Journal of the Korean Society for Aeronautical and Space Sciences 2004; 33 (5): 18-27.
[6] Im YH, Chang KS. Flow Analysis of a Three-Dimensional Airfoil in Ground Effect. Journal of the Korean Society for Aeronautical and Space Sciences 2000; 29 (5): 1-8.
[7] Kim HJ, Chun HH. Design of 2-Dimensional WIG Section by a Nonlinear Optimization Method. J. of the Society of Naval Architects of Korea 1998; 35 (3): 50-59.
[8] Yakhot V., Orszag SA., Thangam S., Gatski TB, Spezoale CG. Development of Turbulent Models for Shear Flows by a Double Expansion Technique. Physics Fluids A 1992; 4 (7): 1510-1520.
[9] STAR-CD v3.15 Methodology. Computational Dynamics, Co.: London. U. K, 2001.
[10] Patankar SV. Numerical Heat Transfer and Fluid Flow. Hemisphere Publication Corporation: 1980.
[11] Poloni AC., Giurgevich A., Onesti L, Pediroda V. Hybridization of a Multi-Objective Genetic Algorithm, a Neural Network and a Classical Optimizer for a Complex Design Problem in Fluid Dynamics. Dipartimento di Energetica Universita di Trieste: Italy, 1999.
[12] Goldberg D. Genetic Algorithms in Search, Optimization and Machine Learning. Addision-Wesle: 1989.
[13] Booker LB. Improving Search in Genetic Algorithms in Davis L(Editor). Genetic Algorithms and Simulated Annealing. Morgan Kaufmann Publishers: Los Altos, CA: 1987.
[14] Staufenbiel RW. On the Design of Stable Ram Airfoil Vehicles. The Royal Aeronautical Society Symposium Proc. 1987; 110-136.
[15] Fink MP., Lastinger JL. Aerodynamic Characteristics of Low-Aspect-Ratio Wings in Close Proximity to the Ground. NASA TN D-926: 1961.
[16] Carter AW. Effect of Ground Proximity on the Aerodynamic Characteristics of Aspect-Ratio-1 Airfoils with and without End Plate. NASA TN D-970: 1961.